IEEE Open Journal of the Computer Society

Received 24 August 2024; revised 21 September 2024; accepted 28 October 2024. Date of publication 25 November 2024; date of current version 13 February 2025. The review of this article was arranged by Associate Editor Jingcai Guo.

Digital Object Identifier 10.1109/OJCS.2024.3492698

IGFU: A Hybrid Underwater Image Enhancement Approach Combining Adaptive GWA, FFA-Net With USM

XIN YUAN [1], CHENHUI WANG[1], XIAOHONG CHEN[1], MINGXUAN WANG[1], NING LI [2] (Member, IEEE), AND CHANGLI YU [1]

[1]School of Ocean Engineering, Harbin Institute of Technology, Harbin 150001, China
[2]School of Computer Science and Technology, Harbin Institute of Technology, Harbin 150001, China

CORRESPONDING AUTHORS: NING LI; CHANGLI YU (e-mail: li.ning@upm.es; yuchangli@hitwh.edu.cn).

This work was supported in part by the National Natural Science Foundation of China (Youth Project) under Grant 62101159, in part by the Chinese Shandong Provincial Natural Science Foundation (General Program) under Grant ZR2021MF055, and in part by Chinese Shandong Provincial Key Research and Development Plan, under Grant 2021CXGC010702, Grant 2022CXGC020410, and Grant 2022CXGC020412.

ABSTRACT To address the issue of color distortion and blurriness in underwater imageries, a hybrid Underwater Image Enhancement (UIE) method combining Adaptive Gray World Algorithm (GWA), Feature Fusion Attention Network (FFA-Net) and Unsharp Masking (USM) is proposed in this research. This method begins with color correction by applying different stretching processes to the RGB components based on the image's color information, and iteratively corrects the colors. Next, the corrected image undergoes dehazing via FFA-Net to eliminate underwater haze and improve clarity. Ultimately, USM is applied to amplify high-frequency components, thus enhancing edge details. Qualitative and quantitative comparisons demonstrate that the proposed Improved GWA FFA-Net USM (IGFU) method outperforms existing techniques in underwater image quality.

INDEX TERMS FFA-Net, GWA, UIE, USM.

I. INTRODUCTION

With the continuous expansion of aquaculture, the operational model of manual diving for seafood increasingly falls short of meeting the requirements for sustainable marine economic development. Not only does artificial fishing incur high labor costs, but it also carries significant safety risk. Therefore, it is a crucial direction for the development of seafood aquaculture to utilize underwater vehicles for automated detection and catching of seafood. Underwater images suffer from poor quality due to seawater's absorptive and scattering effects on light [1]. As illustrated in Fig. 1, seawater selectively absorbs visible light, causing color bias: red light is absorbed first, followed by green, while blue light penetrates the deepest, resulting in a blue-green tint. Scattering further degrades image clarity and contrast, blurring edges and creating a haze effect.

Consequently, underwater images exhibit reduced contrast, color distortion and blurred details, these problems result in insufficient target identification information, which poses a significant obstacle to the detection of marine life. Despite advancements in high-tech underwater imaging equipment,

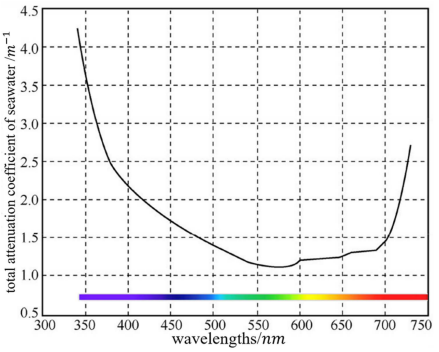

FIGURE 1. Relationship between the total attenuation coefficient of seawater and wavelength.

© 2024 The Authors. This work is licensed under a Creative Commons Attribution 4.0 License. For more information, see https://creativecommons.org/licenses/by/4.0/

the quality of obtained images has been somewhat improved. However, difficulties like color degradation, low contrast and blurred details persist. In addition, the cost of practical application should be considered as well. Therefore, it is still essential to enhance images obtained by underwater vision systems.

Existing UIE technologies can be categorized into three types based on their underlying principles: non-physical model-based methods, physical model-based approaches and those utilizing deep learning technique [2]. Non-physical model-based approaches typically rely on image processing techniques rather than simulating the physical processes of underwater optics [3]. The main principle is to utilize mathematical algorithms and statistical methods to manipulate images, improving contrast, brightness and detail. Common techniques include Histogram Equalization (HE) [4], Contrast Limited Adaptive Histogram Equalization (CLAHE) [5], wavelet transforms [6], white balance [7], etc. These methods do not consider the physical model of underwater light propagation but directly modify image pixel values to increase the visual impact [8]. Physical model-based solutions aim to simulate the physical processes of underwater light propagation, including light attenuation, scattering, refraction, etc. And then design algorithms to compensate for these effects to restore underwater images more accurately [9]. Deep learning methods leverage neural networks and other deep learning models to learn features and patterns of underwater images. They usually require large amounts of labeled data for training and then can be used to repair or improve underwater images [10].

The main contributions of this presented work are summarized as follows:

- A hybrid UIE method is proposed, which combines improved GWA, FFA-Net and USM. It significantly improves image enhancement outcomes and effectively tackles diverse underwater environments.
- An improved GWA is developed, which extracts color information from images and employs an iterative processing approach to adaptively correct underwater image colors. It effectively addresses the over-correction issue of traditional GWA in red tones.
- Three different underwater image datasets are utilized for model training, which successfully extends the application range of FFA-Net from above water to underwater contexts.

The framework structure of this manuscript is arranged as follows. The next section briefly discusses the relevant research and related developments in UIE; Section III introduces the theoretical background of the proposed approach; An IGFU method based on improved GWA is proposed in Section IV; Section V provides a qualitative and quantitative comparison of various UIE methods across different datasets, along with ablation studies that highlight the essential roles of each module in the IGFU approach; finally, Section VI summarizes the entire work and suggests directions for future research.

II. RELATED WORKS

The existing non-physical models for UIE adjust pixel values to improve visual quality but often struggle with severely degraded images and complex environments. Iqbal et al. [11] proposed an Unsupervised Color Correction Method (UCM) that uses RGB and HSI color models for better color accuracy and contrast. Voronin et al. [12] introduced a frequency domain approach with logarithmic transformations and equalization, guided by Enhancement Measure Evaluation (EME), proving effective compared with classical techniques. [13] combined CLAHE and Total Generalized Variation (TGV) for color correction and edge preservation, while [14] developed the Hybrid Fusion Method (HFM) with comprehensive modules for color correction and visibility enhancement. Yang Yicun [15] integrated color correction with local USM for improved color and contrast. However, these methods often fail to effectively address noise, artifacts and varying underwater conditions.

The physical model-based image enhancement methods use mathematical modeling of underwater light propagation to invert the image degradation process, thereby correcting color distortion and contrast issues. Drews et al. [16] developed the UDCP algorithm, improving transmission map estimation and color representation. Li et al. [17] addressed light attenuation with adaptive color restoration and dehazing, enhancing color restoration and increasing the accuracy of underwater target detection. Authors in [18] combined physical and geometric principles, using the Beer-Lambert law to assess light attenuation and geometric algorithms to improve color and detail. [19] introduced a UIE strategy with transmission optimization and Principal Component Analysis (PCA) for background light estimation. Despite their effectiveness, these methods face challenges in generalization, real-time performance and adaptability to diverse underwater scenes.

Deep learning methods significantly advance UIE through automated feature extraction and hierarchical processing. Convolutional Neural Networks (CNNs) like UWCNN [20] and Water-Net [21], [30], [55], Generative Adversarial Networks (GANs) like COC-UFGAN [22] and conditional GAN-based models [23], solves color distortion and contrast issues efficiently. UWCNN directly reconstructs clear images by bypassing traditional parameter estimation steps, while Water-Net integrates various architectures for improved image quality. COC-UFGAN uses color adversarial channels for superior color restoration, and recent conditional GAN models enhance inference speed and reduce memory consumption. Additionally, method combining Adaptive Standardization Network (ASNet) and Adaptive Normalization Network (AN-Net) [24] optimize image contrast and brightness, showing excellent performance in underwater imaging.

III. THEORETICAL BACKGROUND

A. GWA

The selective absorption of visible light by seawater leads to an underwater image's color bias towards green and blue hues,

FIGURE 2. Underwater images processed by GWA.

resulting in color distortion. Therefore, to enhance underwater imagery, it is imperative to first correct the color bias in the images. This initial step is crucial for obtaining more accurate information about subsea environment, like underwater organisms and reefs.

GWA [52], [53] is a prevalent method for color correction in underwater imaging, offering substantial improvements in the correction of color distortions in imageries affected by underwater conditions [25].

While the GWA can correct color in underwater images [59], in cases where the color distribution is uneven, the color deviation is significant, and specific colors dominate. It is quite possible that the color correction will be erroneous [57], causing the colors in the image distorted again. In the underwater environment, red light attenuates most severely, resulting in the grayscale value of the red channel in underwater images being much lower than that of the blue and green channels [54]. When the GWA is applied to adjusting the average color of the image to neutral gray, the algorithm excessively enhances the red channel to compensate for the lack of red light. This compensation often leads to an oversaturation of red components in the image, resulting in overcorrection [35].

To validate the conclusions, 50 characteristic underwater images were selected from the UIEB dataset [27], [29], [30], [31], [32], [33], [34], [35], [36], [37], [38], [39], [40] to form a test set, and corresponding reference images were extracted from the UIEB dataset as a validation set. The UICM [60] and CCF_colorfulness [45] metrics were employed as quantitative indicators to assess the color correction performance of the traditional GWA in Fig. 2. The results indicate that the GWA can reduce the color difference in underwater images to some extent, but it is accompanied by a noticeable over-correction of red, and there remains a gap in color correction effectiveness compared with that of the reference images.

In response to the issue of red channel overcorrection produced by the traditional GWA and considering the unique characteristics of color channels in underwater environments, an improved GWA is proposed. It is capable of adaptively correcting colors in underwater images and circumventing the problem of red overcorrection. When combined with a dehazing network, it yields underwater enhanced images with superior visual effect.

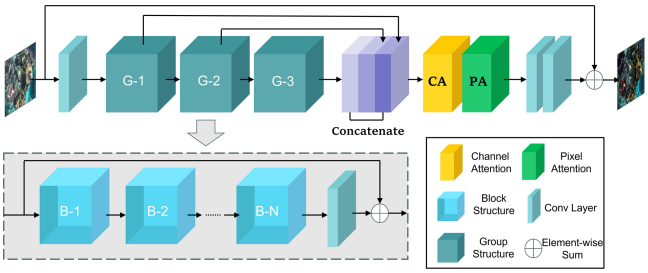

FIGURE 3. FFA-Net network structure diagram.

B. FFA-NET

Due to the backward scattering of light by seawater, underwater images often exhibit reduced sharpness and contrast, resulting in a hazy appearance that significantly compromises image quality. To counteract this effect, dehazing neural networks can be applied to underwater imagery to dispel the haze, thus enhancing both contrast and clarity, besides elevating the overall quality and visual experience of the image.

1) MODEL STRUCTURE

FFA-Net was proposed in 2020 [26], which can keep the shallow information of the image, sends it to the deeper layers, and gives different weights to features at various levels based on adaptive learning, ultimately achieving dehazing task. The FFA network, as shown in Fig. 3, starts with a hazy underwater image input. This image undergoes shallow feature extraction, followed by processing through N Group Architectures with skip connections. The resultant features are combined by a Feature Attention (FA) module and finally reconstructed into a haze-free image through a global residual learning structure.

2) FA

FA in image dehazing networks differentiates between channel and pixel features, offering adaptability for diverse information and enhancing CNNs' representational capacity. FA's channel attention and pixel attention components allow for unequal treatment of features, addressing the challenge of uneven fog distribution in images.

In terms of Channel Attention (CA), it is completely diverse weighted information of different channel features paid attention to in DCP [27]. First, global average pooling is applied to integrating the global spatial information of the channel into a channel descriptor.

$$g_c = H_p(F_c) = \frac{1}{H \times W} \sum_{i=1}^{H} \sum_{j=1}^{W} X_c(i, j) \tag{1}$$

where $X_c(i, j)$ represents the value of the c-th channel X_c at position (i, j), and H_p is the global pooling function. The shape of the feature map changes from $C \times H \times W$ to $C \times H \times 1$. To obtain weights for different channels, the features pass through two layers of convolutional layers and sigmoid and ReLU activation functions.

$$CA_c = \sigma(Conv(\delta(Conv(g_c)))) \tag{2}$$

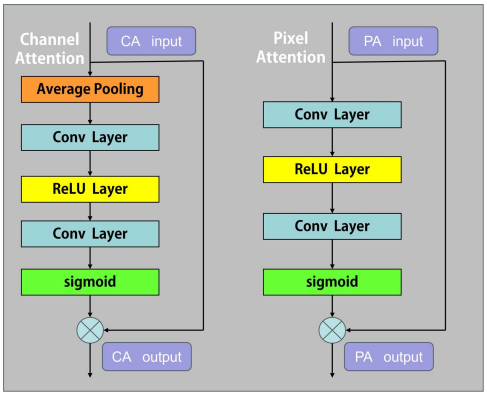

FIGURE 4. The diagram of CA and PA structure.

where σ is the sigmoid function, δ is the ReLU function. Finally, element-wise multiplication is performed between the input F_c and the weights of channel CA_c.

$$F_c^* = CA_c \otimes F_c \tag{3}$$

In terms of PA, considering that the distribution of fog is uneven across different image pixels, a PA module is presented that allows the network to pay more attention to information-rich features, such as thick-hazed pixels and high-frequency image regions.

Like CA, the input F^* (the output of the CA) is directly fed into two convolution layers with ReLU and sigmoid activation functions. The shape changes from $C \times H \times W$ to $1 \times H \times W$.

$$PA = \sigma\left(Conv\left(\delta\left(Conv\left(F^*\right)\right)\right)\right) \tag{4}$$

Lastly, element-wise multiplication is employed between the input F^* and PA, $\tilde{F}$ is the output.

$$\tilde{F} = F^* \otimes PA \tag{5}$$

This ensures that the model focuses on significant regions while suppressing less informative ones.

3) BASIC BLOCK STRUCTURE

The basic block structure in Fig. 4 cleverly combines local residual learning and the FA module. The FA module dynamically prioritizes crucial feature channels, while local residual learning skips unimportant information, reducing redundancy and loss. This design boosts FFA-Net's underwater image dehazing performance, stabilizes training, and enhances feature extraction, resulting in clearer and more detailed dehazed images.

4) GROUP ARCHITECTURE AND GLOBAL RESIDUAL LEARNING

The group architecture in FFA-Net is pivotal, integrating multiple basic blocks with skip connections, enhancing network depth and feature representation for versatile defogging tasks. Skip connections bypass non-essential data, streamlining the transfer of key information to deeper layers, mitigating training challenges and enhancing model generalization. The network's recovery section, featuring convolutional layers and a global residual module, refines features and preserves image details for high-quality defogging outcomes.

IV. THE PROPOSED IGFU METHOD

The presented IGFU approach primarily encompasses three components: the Improved GWA, the FFA-Net dehazing network and USM. Initially, the underwater image undergoes color correction via the improved GWA. Subsequently, the preprocessed image is input into the FFA-Net dehazing network for haze removal. Finally, the image is subjected to USM to enhance its details. This approach effectively corrects color cast in images, enhances edge details and improves image contrast and clarity, thereby raising the quality and visual perception of underwater imagery.

Distinguished from the three common types in the UIE approach, the method presented in this manuscript is a hybrid fusion-based UIE method that integrates color correction algorithm with deep learning. In contrast to other hybrid methods that enhance underwater image quality by combining color balancing algorithms with image fusion techniques [14], this work first analyzes three types of quality defects present in underwater images and adopts different processing methods for each distinct defect, thereby achieving more targeted image quality enhancement. Furthermore, the existing improved GWA is primarily used to address the limitations of the traditional GWA, which may be ineffective in images with fewer colors [57] and large dominant color blocks [58], primarily used for processing terrestrial images. The improved GWA, however, is mainly applied to the field of color correction for underwater images. By extracting color information and the color characteristics of underwater images, it performs color correction in a self-adaptive manner. The improved GWA not only solves color cast issues, but also addresses the algorithm failure caused by large areas of blue and green color blocks.

A. IMPROVED GWA

Due to seawater's significantly greater absorption of red light compared with blue and green light, the intensity of the red channel in underwater images is markedly low. The conventional GWA, when applied to underwater images, tends to excessively stretch the red channel, leading to an overcorrection of red hues. The traditional Gray World framework is built by incorporating multiple judgment parameters and conditions from various image processing stages, coupled with the concept of iterative processing, a segmented linear stretching approach is proposed to individually process each of the three-color channels, thereby resolving the issue of red overcorrection during the color correction process. Simple linear stretching is performed separately on three color channels [35].

$$C_{\text{new}} = \begin{cases} \frac{C_{\min}-128}{C_{\min}-\bar{C}} \times \left(C-\bar{C}\right)+128, & \bar{C} \le 128 \\ \frac{C_{\max}-128}{C_{\max}-\bar{C}} \times \left(C-\bar{C}\right)+128, & \bar{C} > 128 \end{cases} \tag{6}$$

where C represents the values of the R, G, B color channels. C_{new} denotes the value of the C channel after processing. $C_{\min}$ and $C_{\max}$ are respectively the minimum and maximum values of the C channel, while $\bar{C}$ signifies the average value of the C channel.

Common underwater images mainly present two-color tones that are blue and green. Thus, in the next processing phase, distinct methodologies will be adopted for the correction of underwater images exhibiting blue and green biases. This bespoke approach ensures that the color correction algorithm is finely attuned to the distinct optical characteristics exhibited by each type of chromatic aberration, facilitating an adaptive treatment across various underwater imaging conditions.

The proportional coefficients are introduced for the R, G, B channels as P_r, P_g, P_b; the correction coefficients for the R, G, B channels are λ_r, λ_g, λ_b; the relationship coefficient between the red and green channels is M, and between the red and blue channels is N; the channel intensity threshold is P, and the average grayscale value of the channels is K_{avg}.

The proportion coefficients P_r, P_g and P_b represent the proportion of pixel grayscale values in the R, G, B channels that are less than the channel intensity threshold P. By evaluating the magnitude of these proportion coefficients for each channel, the quantity of low grayscale value pixels can be determined in that channel, which serves as the basis for deciding whether to perform a mild correction on that channel. If the proportion coefficients for each channel exceed a certain value, it is inferred that the pixels in that channel are primarily distributed in the low grayscale value area, the channel average value is small, and the color distribution is uneven. Consequently, direct application of the piecewise linear processing described in (6), which stretches the channel's average grayscale value to 128 is not advisable. Instead, a mild stretching treatment should be performed on this channel based on the correction coefficients λ_r, λ_g, λ_b to avoid overcorrection. Conversely, when the proportion coefficient of the channel is small, normal linear stretching processing is performed on the channel. The specific mild correction expression is:

$$\begin{cases} R_{new} = R - \lambda_r \times \left(\bar{R} - 128\right), & P_r > 0.6 \\ G_{new} = G - \lambda_g \times \left(\bar{G} - 128\right), & P_g > 0.6 \\ B_{new} = B - \lambda_b \times \left(\bar{B} - 128\right), & P_b > 0.6 \end{cases} \tag{7}$$

where $\bar{R}$, $\bar{G}$ and $\bar{B}$ indicate the average values of the red, green and blue channels, individually. R_{new}, G_{new} and B_{new} represent the intensity values of the corrected red, green and blue channel components, respectively. The specific expressions for the correction coefficient (λ_r, λ_g, λ_b) and the proportion coefficient (P_r, P_g, P_b) are:

$$P_r = \frac{n_r}{N},\ P_g = \frac{n_g}{N}, P_b\ = \frac{n_b}{N} \tag{8}$$

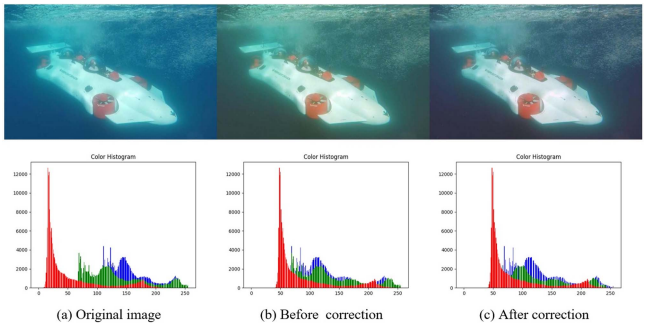

FIGURE 5. The effect after attenuated correction of the green channel.

$$\begin{cases} \lambda_r = \dfrac{P_r - \frac{|K_{avg} - \bar{R}|}{3 \times K_{avg}}}{P_r + P_g + P_b} \\ \lambda_g = \dfrac{P_g}{P_g + P_b} \\ \lambda_b = \dfrac{P_b}{P_g + P_b} \end{cases} \tag{9}$$

where N is the total number of pixels in the image, and n_r, n_g, n_b represent the number of pixels in the image where the grayscale value is less than the channel intensity threshold P among all pixels.

Given the significantly lower intensity of the red channel in underwater images compared with that of the blue and green channels, the refined algorithm primarily focuses on mitigating overcorrection in the red channel. Post-processing of the red channel results in a reduced average intensity, preventing the occurrence of overcorrected red hues in the image. Nevertheless, if the blue and green channels are processed using the method described in (6), the overall image may exhibit a greenish cast. Therefore, while performing a gentle stretching of the red channel based on correction coefficients, it is also necessary to apply a different treatment on the green channel than that specified in (6) to ensure that the processed image does not display a green bias. The specific method for processing the green channel is:

$$G_{new} = \begin{cases} G - \lambda_g \times (\bar{G} - 128), & P_g > 0.6 \\ \frac{G_{\min} - 128}{G_{\min} - \bar{G}} \times (G - \bar{G}) + 128, & \bar{G} < 128, P_r < 0.6 \\ \frac{G_{\min} - 128}{G_{\min} - \bar{G}} \times (G - \bar{G}) + 128 - \frac{|\bar{B} - \bar{G}|}{2}, & \bar{G} < 128, P_r > 0.6 \\ \frac{G_{\max} - 128}{G_{\max} - \bar{G}} \times (G - \bar{G}) + 128, & \bar{G} \geq 128, P_r < 0.6 \\ \frac{G_{\max} - 128}{G_{\max} - \bar{G}} \times (G - \bar{G}) + 128 - \frac{|\bar{B} - \bar{G}|}{2}, & \bar{G} \geq 128, P_r > 0.6 \end{cases} \tag{10}$$

where $G_{\min}$ and $G_{\max}$ are the minimum and maximum values of the G channel, separately. In Fig. 5, by concurrently applying a mild correction to the red channel and an attenuated correction to the green channel, the issue of the image exhibiting a greenish bias can be avoided.

As indicated by the histogram in subfigure (c) of Fig. 5, compared with the histogram in subfigure (b), the intensity of

the green channel is reduced after the attenuated correction, preventing the image from displaying a greenish appearance. Thus, the attenuated correction of the green channel enables the processed image to retain more authentic and natural colors.

The coefficients M and N reflect the relationship between the intensity of the red channel and that of the blue and green channels, respectively. The average grayscale value K_{avg} is the mean of the sum of the average grayscale values of the three channels. The specific expressions are:

$$M = \frac{\bar{R}}{\bar{G}}, \quad N = \frac{\bar{R}}{\bar{B}}, \quad K_{avg} = \frac{\bar{R}+\bar{G}+\bar{B}}{3} \tag{11}$$

The grayscale range of an image is segmented into three distinct zones: low, medium and high. The channel intensity threshold P serves as the demarcation value that separates the low grayscale values from the medium grayscale values within this range. As illustrated in Fig. 6, the original image's average channel grayscale value $K_{avg} = 46.5,\ 46.8,\ 126.3$; subfigure (b) demonstrates the effect when P is 55, while (c) displays the result when P is an adaptive value. For underwater images with a green bias ($\bar{G} \geq \bar{B}$), the method for determining the value of P is:

$$P = \begin{cases} K_{avg} \times 0.8, & K_{avg} < 55 \\ \frac{1}{9} K_{avg} + 47, & 55 \leq K_{avg} \leq 100 \\ K_{avg} \times 0.2, & 100 < K_{avg} \leq 120 \ \& \ M \leq 0.2 \\ K_{avg} \times M, & 100 < K_{avg} \leq 120 \ \& \ 0.2 < M < 0.7 \\ K_{avg} \times 0.7, & 100 < K_{avg} \leq 120 \ \& \ M \geq 0.7 \\ K_{avg} \times 0.2, & 120 < K_{avg} \ \& \ M \leq 0.2 \\ K_{avg} \times M, & 120 < K_{avg} \ \& \ 0.2 < M < 0.7 \\ K_{avg} \times 0.7, & 120 < K_{avg} \ \& \ M \geq 0.7 \end{cases} \tag{12}$$

For underwater images with a blue bias ($\bar{G} < \bar{B}$), the method for determining the value of P is:

$$P = \begin{cases} K_{avg} \times 0.8, & K_{avg} < 55 \\ K_{avg} \times 0.4, & 55 \leq K_{avg} \leq 100 \ \& \ N \leq 0.2 \\ K_{avg} \times \left(\frac{4}{5}N + 0.34\right), & 55 \leq K_{avg} \leq 100 \ \& \ 0.2 < N < 0.7 \\ K_{avg} \times 0.8, & 55 \leq K_{avg} \leq 100 \ \& \ N \geq 0.7 \\ K_{avg} \times 0.4, & 100 < K_{avg} \leq 120 \ \& \ N \leq 0.2 \\ K_{avg} \times \left(\frac{4}{5}N + 0.34\right), & 100 < K_{avg} \leq 120 \ \& \ 0.2 < N < 0.7 \\ K_{avg} \times 0.8, & 100 < K_{avg} \leq 120 \ \& \ N \geq 0.7 \\ K_{avg} \times 0.4, & K_{avg} > 120 \ \& \ N \leq 0.2 \\ K_{avg} \times \left(\frac{4}{5}N + 0.34\right), & K_{avg} > 120 \ \& \ 0.2 < N < 0.7 \\ K_{avg} \times 0.8, & K_{avg} > 120 \ \& \ N \geq 0.7 \end{cases} \tag{13}$$

The determination of P's value will dictate the magnitude of the proportional coefficients, thereby influencing the outcome of subsequent color correction. Compared with setting P as a fixed value, the method of adaptively obtaining P is valid and offers a superior correction effect.

It is apparent that the color correction is significantly more effective when P is an adaptive value rather than a fixed one.

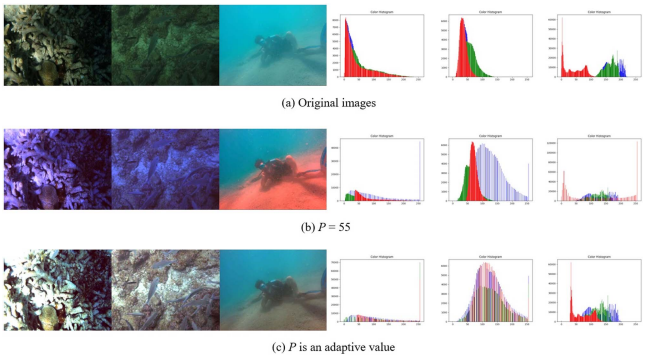

FIGURE 6. Results and histograms of the improved GWA when P is a fixed value and an adaptive data.

When the average grayscale value of the image's channels is low (dark image), setting P as a constant data of 55 can mislead the computer into believing that the intensity of each channel is predominantly in the lower grayscale value region, with an average channel value less than others, suggesting an uneven color distribution. In summary, the improved processing methods for the R, G, B channels are as follows:

$$R_{new} = \begin{cases} R - \lambda_r \times (\bar{R} - 128), & P_r > 0.6 \\ \frac{R_{\min}-128}{R_{\min}-\bar{R}} \times (R - \bar{R}) + 128, & \bar{R} < 128 \\ \frac{R_{\max}-128}{R_{\max}-\bar{R}} \times (R - \bar{R}) + 128, & \bar{R} \geq 128 \end{cases}$$

$$G_{new} = \begin{cases} G - \lambda_g \times (\bar{G} - 128), & P_g > 0.6 \\ \frac{G_{\min}-128}{G_{\min}-\bar{G}} \times (G - \bar{G}) + 128, & \bar{G} < 128, P_r < 0.6 \\ \frac{G_{\min}-128}{G_{\min}-\bar{G}} \times (G - \bar{G}) + 128 - \frac{|\bar{B}-\bar{G}|}{2}, & \bar{G} < 128, P_r > 0.6 \\ \frac{G_{\max}-128}{G_{\max}-\bar{G}} \times (G - \bar{G}) + 128, & \bar{G} \geq 128, P_r < 0.6 \\ \frac{G_{\max}-128}{G_{\max}-\bar{G}} \times (G - \bar{G}) + 128 - \frac{|\bar{B}-\bar{G}|}{2}, & \bar{G} \geq 128, P_r > 0.6 \end{cases}$$

$$B_{new} = \begin{cases} B - \lambda_b \times (\bar{B} - 128), & P_b > 0.6 \\ \frac{B_{\min}-128}{B_{\min}-\bar{B}} \times (B - \bar{B}) + 128, & \bar{B} < 128 \\ \frac{B_{\max}-128}{B_{\max}-\bar{B}} \times (B - \bar{B}) + 128, & \bar{B} \geq 128 \end{cases} \tag{14}$$

where R_{new}, G_{new} and B_{new} denote the intensity values of the corrected red, green and blue channel components, respectively. $R_{\min}$, $R_{\max}$, $G_{\min}$, $G_{\max}$, $B_{\min}$, $B_{\max}$ are the minimum and maximum values of the R, G and B channels.

The improved GWA can effectively circumvent the overcorrection phenomenon predominantly observed in the red channel. However, due to the reduction in the intensity stretching of the red channel, the disparity between the processed image and the original is not substantial for certain images. Therefore, embracing the concept of iterative processing and making full use of the color channel information of the image, iterative determination parameters δ_1, δ_2, δ_3 are introduced, as demonstrated in (15):

$$\delta_1 = \frac{\bar{R}}{K_{avg}}, \quad \delta_2 = \frac{(\bar{R}_{new} - \bar{R})}{\bar{R}}, \quad \delta_3 = \delta_1 + 0.12 \times \delta_2 \tag{15}$$

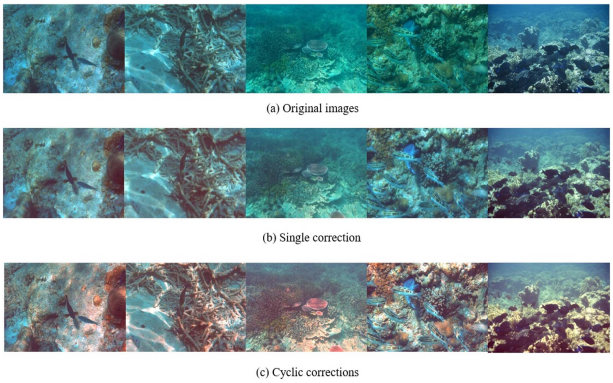

FIGURE 7. The results of image processing after a single correction and cyclic corrections.

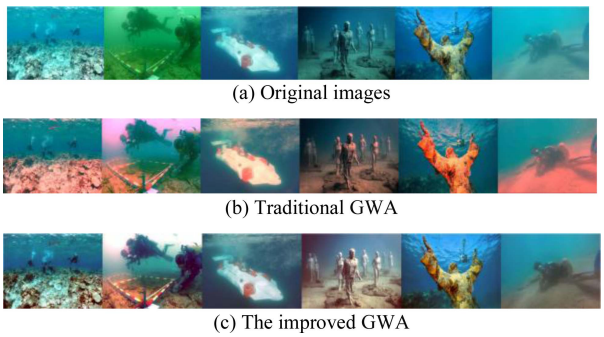

FIGURE 8. Comparative results of the improved GWA and the traditional GWA.

where $\bar{R}_{new}$ represents the average vals of the corrected red channel components. When the following criteria are satisfied, the underwater image is subjected to an iterative process by the proposed method.

$$\begin{cases} 0.1 \times \delta_2 > 0.07 \; or \; \delta_1 > 0.55 \\ \delta_1 > 0.05 \\ \delta_3 > 0.5 \end{cases} \tag{16}$$

The results of color correction using the proposed method, with a single iteration and multiple cycles, are illustrated in Fig. 7. It is evident that some images subjected to a solitary color correction process (b) still exhibit a bias towards blue and green hues. By contrast, the images that have undergone cyclic processing (c) display vibrant colors and a markedly improved correction effect.

All in all, compared with the conventional GWA, the improved algorithm effectively addresses the issue of over-correction in red tones. It provides a robust correction for the overall color cast of the image, enhances the brightness of underwater images, and restores their true colors, resulting in a superior visual effect. The specific processing results are illustrated in Fig. 8.

B. FFA-NET TRAINING AND TESTING

The underwater sea cucumber image dataset is selected from Shandong Future Technology Robotics Company Ltd. [28] and the open-source UIEB dataset as the sources for training set. A total of 225 images are selected from these datasets and divided into a training set and a test set in a 7:3 ratio. To demonstrate the universality of the network, the selected images include but are not limited to clear, blurry, blue-biased, green-biased, misty and heavily foggy types. Additionally, random rotations are performed (including 90 degrees, 180 degrees and 270 degrees) and horizontal flips on the images in the training dataset to augment the data. This helps the network learn more comprehensive feature representations, thereby improving the generalization and robustness of FFA-Net.

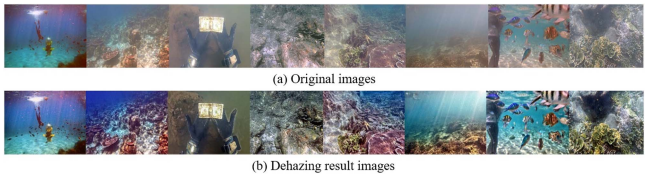

FIGURE 9. Comparison of Original images and Dehazing result images.

The FFA-Net is trained on RGB channels. To unify the dataset specifications and accelerate network training speed, the input images are resized to 256 × 256. The network is trained for 2.25×10^5 steps, with a learning rate of 1×10^{-4}. The Adam optimizer is utilized for adaptive learning rate optimization, with $\beta 1$ and $\beta 2$ setting to their default values of 0.9 and 0.999. The learning rate adjustment adopted a cosine decay strategy [41], gradually reducing it from the initial learning rate 0. The specific calculation formula is:

$$\eta_t = \frac{1}{2}\left(1 + \cos\left(\frac{t\pi}{T}\right)\right)\eta \tag{17}$$

where T is the total number of batches, η is the initial learning rate, and t is the current batch.

The PyTorch [42] framework and RTX 3090 are applied to train the network model. The trained network model is imported into the specified path and selected the images that have undergone the first step of improved GWA processing as test data. The comparison of the results is displayed in Fig. 9.

It is evident that compared with the original images, the foggy regions in the images processed by FFA-Net are largely eliminated, besides the clarity and contrast are significantly improved.

C. USM PROCESSED IMAGES

Following the processing by the improved GWA and the FFA-Net dehazing network, the underwater image's color accuracy was effectively corrected, and there was a notable enhancement in the image's clarity and contrast, with the foggy effect being removed. However, the problem of image detail blurring due to the scattering of light by seawater was not resolved. Therefore, it is necessary to apply USM to the image post the initial two steps of processing to achieve an image with intensified details.

USM primarily operates by subtracting an image that has been smoothed with a low-pass filter from the original image,

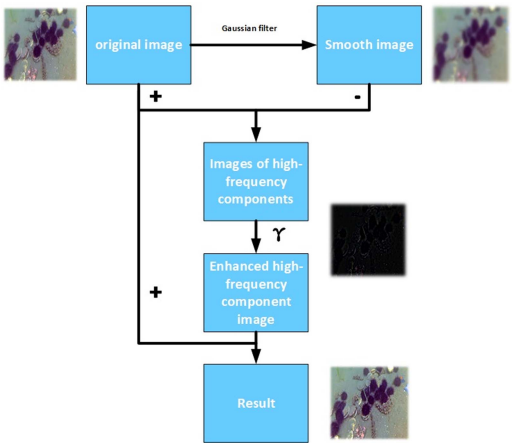

FIGURE 10. The implementation steps of USM.

thereby isolating the high-frequency components that accentuate the fine details within the image. These high-frequency elements are then reintroduced into the original image at a certain ratio, enhancing the image's sharpness and the definition of its edges [56]. This technique effectively amplifies the minute details that contribute to visual perception. The process flowchart for image processing using USM is in Fig. 10.

Initially, the underwater image is subjected to Gaussian blurring to remove high-frequency details and noise, obtain a blurred image representing the low frequency components. The blur is defined by a Gaussian function with a standard deviation σ, the expression of Gaussian function $G(x, y)$ is:

$$G(x, y) = \frac{1}{2\pi\sigma^2} e^{-\frac{x^2+y^2}{2\sigma^2}} \tag{18}$$

where σ represents the standard deviation within the Gaussian blur, determining the breadth of the Gaussian function and consequently influencing the degree of blurring. The size of the Gaussian kernel, also referred to as the filter, is typically selected based on the value of σ. A smaller σ yields a subtler blur effect, as the Gaussian kernel predominantly affects pixels near the center. Conversely, a larger σ value extends the kernel's influence over a broader pixel area, resulting in a more pronounced blurring effect.

Subsequently, by subtracting the smoothed image from the original image, a detail image predominantly containing high-frequency information is obtained.

Finally, the detailed image is multiplied by a sharpening intensity (typically a value greater than 1), and this enhanced detail image is then added to the original one, yielding the final enhanced image. The mathematical expression for the method is:

$$H = R + \gamma R - G(x, y) \times R \tag{19}$$

where H is the result, R is the input, $G(x, y)$ is the Gaussian filter, γ is the sharpening intensity. The processed result is displayed in Fig. 11.

FIGURE 11. Enhancement of underwater image details by using USM.

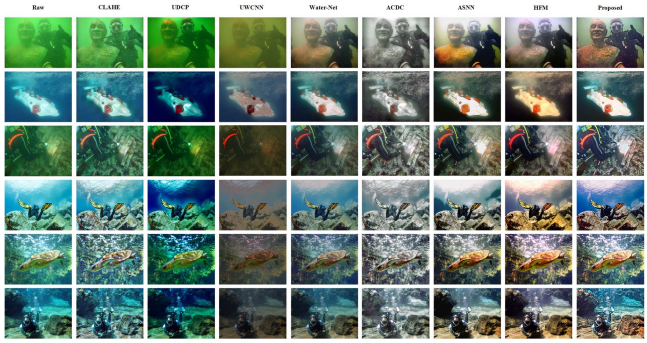

FIGURE 12. Images processed by different methods on the UIEB dataset.

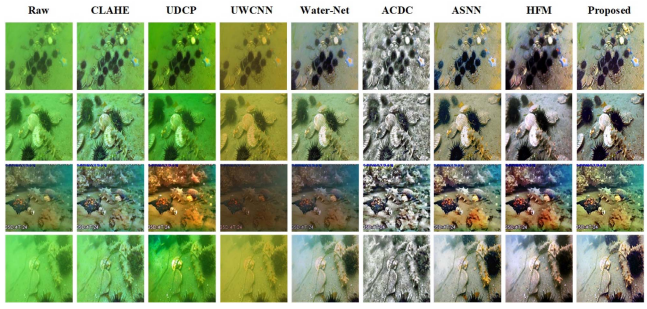

FIGURE 13. Images processed by different methods on the sea cucumber dataset.

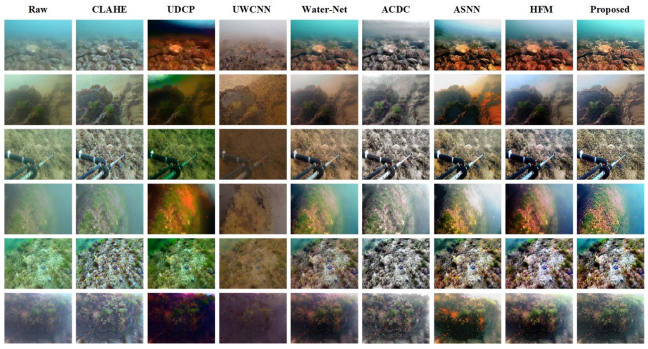

FIGURE 14. Images processed by different methods on the UIDEF dataset.

After applying the USM, there is a significant enhancement in the image's details. The edges become more defined, and the features are more pronounced.

V. EXPERIMENTS RESULTS WITH RELEVANT ANALYSIS

A. EXPERIMENTAL SETTINGS

To train FFA-Net and compare IGFU with various UIE methods, three datasets were used for network training, image testing and analysis:

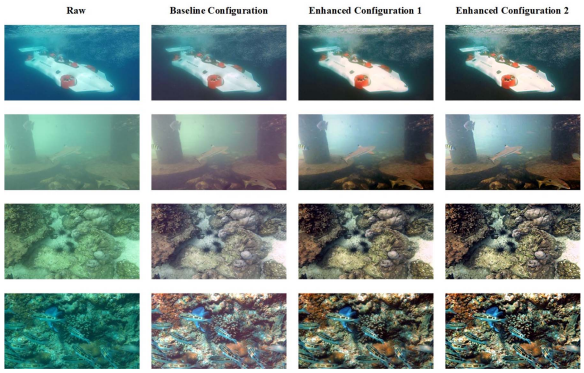

FIGURE 15. Images processed by different configurations on the UIEB dataset.

TABLE 1. Color Quantitative Evaluation Index Results of Gwa

	UICM ↑	CCF_colorfulness ↑
Raw	8.9166	38.3068
GWA	11.9583	53.5683
Reference	13.9989	72.0277

- UIEB: An open-source dataset with 950 authentic underwater images and 890 high-quality reference images, encompassing diverse types of seawater, depths, lighting conditions and scene content.
- UIDEF: An extensive dataset with 9200 real-world underwater images across 7 categories and 11 subcategories [48]. These categories broadly cover various common degradation types in underwater imagery and different shooting perspectives.
- Sea Cucumber Dataset: Covers various types of seawater, lighting conditions, biological quantities and shooting angles, totally contains 3117 images of sea cucumbers in both above-water and underwater scenarios, sourced from Shandong Future Technology Robotics Company Ltd [28].

For training FFA-Net, 225 images from UIEB and the sea cucumber dataset were selected and divided into training (70%) and testing (30%) sets, with data augmentation applied. The selected images include but are not limited to clear, blurry, blue-tinted, green-tinted, foggy and heavy mist types. The training dataset underwent random rotations (including 90 degrees, 180 degrees and 270 degrees) and horizontal flips to augment the data.

The test set included 100 images from UIEB, 100 from each UIDEF category and 50 from the sea cucumber dataset to evaluate the performance of various UIE methods.

FFA-Net was trained under the experimental environment configuration shown in the Table 2.

FFA-Net was trained on RGB channels with input images resized to 256 × 256, a batch size of 4 and trained for 2.25×10^5 steps using an initial learning rate of 1×10^{-4}. The Adam optimizer with default $\beta 1$ and $\beta 2$ values of 0.9 and 0.999 was used, along with a cosine decay learning rate adjustment.

TABLE 2. The Computer Configurations

Items	Version
CPU	Intel(R)Xeon(R) Gold 6230R CPU @ 2.10GHz
GPU	NVIDIA GeForce RTX 3090, 24 GB
RAM	256G
Python	3.11
CUDA	CUDAv12.1
Pytorch	2.2.0

To assess IGFU's effectiveness, seven UIE techniques were compared: two non-physical model-based methods (CLAHE [5]), one physical model-based method (UDCP [16]), two deep learning-based networks (UWCNN [20] and Water-Net [21], [30], [55]) and two recent methods that are Attenuated Color Channel Correction and Detail Preserved Contrast Enhancement (ACDC) [49], Adaptive Standardization and Normalization Networks (ASNN) [24] and HFM [14].

B. QUALITATIVE ANALYSIS

Representative underwater images from the UIEB, sea cucumber and UIDEF datasets, showcasing various color tones, scenes, clarity, lighting and depths were processed using different UIE methods. The qualitative comparison of these algorithms on the UIEB test set is illustrated below.

CLAHE provides effective color correction for images, yet its dehazing capability requires improvement. UDCP-treated images are characterized by significant distortion and an unsatisfactory visual outcome. UWCNN is unable to eliminate the underwater veils, often accompanied by continuous dark patches, color distortion and lower image quality. Water-Net achieves color correction but falls short in dehazing, leading to images with low clarity and indistinct edge details. The images processed by ACDC generally exhibit a grayish hue, with a loss of color information and it is prone to pseudo-contour artifacts. The ASNN-processed images, while offering clear edge details, have an overall yellowish hue, with mediocre defogging capabilities and pseudo-contour artifacts due to inadequate quantization, accompanied by large dark areas. To a certain extent, HFM can enhance the quality of images, effectively restore the color of green-tinted images, and the resulting underwater images exhibit satisfactory visual effects. However, HFM does not effectively enhance the edge details of images. Additionally, when processing images with a blue bias, HFM tends to over-correct the colors, leading to an overall yellowish hue in the processed imageries.

Overall, non-physical model-based algorithms (CLAHE) provide limited color correction and clarity enhancement, some images even exhibit abnormal color distortions. UDCP improves color saturation and contrast but makes images darker and does not effectively remove color cast and underwater veils. UWCNN suffers from poor visual quality and severe distortions. Water-Net achieves some color correction and dehazing but with low brightness and unclear details. ACDC performs well in image dehazing and shows superior color performance on the UIDEF dataset relative to

TABLE 3. Comparison of Average No-Reference Quality Scores for Different Enhancement Methods on the UIEB Dataset

Method	EME ↑	UCIQE ↑	CCF ↑	FDUM ↑	NIQE ↓	CEIQ ↑	NIQMC ↑
CLAHE	16.9940	0.5985	22.7793	0.6371	3.5335	3.3106	5.0610
UDCP	23.5743	**0.6275**	**41.9738**	0.6018	3.8719	2.9741	4.6825
UWCNN	8.3934	0.5202	10.9372	0.3285	4.1263	2.7511	3.6364
Water-Net	12.6579	0.6061	17.4962	0.5026	4.4671	3.2292	4.8464
ACDC	18.1874	0.5581	25.8878	0.4842	**3.3457**	3.5383	5.5319
ASNN	21.0078	0.6230	24.2285	**0.7049**	3.8177	3.4938	5.4714
HFM	**30.9439**	0.6201	32.4958	0.6559	3.6074	**3.5840**	**5.6221**
Proposed	**42.1404**	**0.6508**	**38.0698**	**0.7992**	**3.3934**	**3.5388**	**5.5835**

TABLE 4. Comparison of Average No-Reference Quality Scores for Different Enhancement Methods on the UIDEF Dataset

Method	EME ↑	UCIQE ↑	CCF ↑	FDUM ↑	NIQE ↓	CEIQ ↑	NIQMC ↑
CLAHE	7.7986	0.5321	15.6028	0.3625	4.7015	3.1092	4.4920
UDCP	11.4422	0.5644	**31.9716**	0.4042	5.8268	2.9600	4.3359
UWCNN	5.4713	0.4805	9.5432	0.2154	5.7945	2.8000	3.6873
Water-Net	6.7747	0.5821	13.4912	0.3135	6.9848	3.3591	5.0486
ACDC	11.6863	0.5402	20.3866	0.3300	**4.1915**	3.5424	5.5135
ASNN	14.1836	**0.6012**	19.8913	0.4372	6.3912	**3.5498**	**5.5245**
HFM	**16.9897**	0.6005	26.1862	**0.4433**	5.5560	**3.6144**	**5.5951**
Proposed	**28.5899**	**0.6098**	**27.8727**	**0.5710**	**4.1773**	3.5464	5.5067

TABLE 5. Comparison of Average No-Reference Quality Scores for Different Enhancement Methods on the Sea Cucumber Dataset

Method	EME ↑	UCIQE ↑	CCF ↑	FDUM ↑	NIQE ↓	CEIQ ↑	NIQMC ↑
CLAHE	8.7739	0.4933	17.9059	0.3678	4.1479	2.9356	4.2972
UDCP	9.3716	0.5298	26.5179	0.3826	4.7546	2.9338	4.2250
UWCNN	4.8970	0.4345	10.1837	0.2213	5.5646	2.3986	2.9881
Water-Net	11.8340	0.5578	18.1405	0.4370	4.2938	3.1353	4.6965
ACDC	24.5852	0.5501	**35.3692**	0.4522	**3.6307**	**3.5901**	**5.6864**
ASNN	**27.7757**	0.5960	30.4233	**0.6318**	3.9395	3.4985	5.4368
HFM	27.0983	**0.5964**	33.5973	0.5482	4.1091	**3.5772**	**5.5132**
Proposed	**37.8225**	**0.6154**	**39.6724**	**0.6242**	**3.9236**	3.4781	5.4371

the other two datasets. However, it tends to produce images with monotonous colors, which does not effectively restore the original color. ASNN effectively reduces chromatic aberrations and improves clarity but sometimes introduces a yellowish hue and high contrast issues, resulting in the loss of details in the highlights and difficulty in distinguishing the shadows. Although occasional pseudo-contour and large dark block phenomena occur, the overall visual effect and image quality are quite good. HFM demonstrates significant efficacy in correcting the color of underwater images, thereby enhancing image quality and restoring color information. Despite the subdued definition of image edges and the less satisfactory color adjustment in blue-dominant images, which can result in a yellowish tinge, HFM still manages to enhance the visual quality of underwater images.

By contrast, for various datasets the proposed IGFU method excels in color correction, edge enhancement and dehazing, delivering high-quality images with excellent visual effects that align well with human visual perception.

C. QUANTITATIVE RESULT

The objective image quality of various methods was evaluated on the UIEB, UIDEF and sea cucumber datasets using seven metrics: EME [43], UCIQE [44], CCF [45], FDUM [46], NIQE [47], CEIQ [50] and NIQMC [51]. The results are shown in Tables 3 to 5, the bold red data represent the optimal results, while the bold blue numbers denote the suboptimal ones.

Tables 3 to 5 illustrate that the proposed IGFU approach outperforms other UIE methods, particularly in EME, demonstrating its superior ability to enhance color correction, definition and contrast. In three distinct datasets, the proposed IGFU method consistently achieves the highest EME scores, outperforming the second-ranked algorithm by 36.18%, 68.28%

TABLE 6. Comparison of Average Quantitative Scores for Different Configurations on the UIEB Dataset

Configuration	EME↑	UCIQE↑	CCF↑	FDUM↑	NIQE↓	CEIQ↑	NIQMC↑
BC	12.226	0.618	29.102	0.6413	3.824	3.346	5.106
EC1	18.011	0.638	30.451	0.6576	3.530	3.487	5.433
EC2	**42.140**	**0.651**	**38.070**	**0.7992**	**3.393**	**3.539**	**5.583**

and 36.17%, respectively. This indicates that the underwater images processed by IGFU method exhibit a higher contrast, effectively highlighting the edges and details of the image content. By enhancing the contrast between light and dark areas, IGFU can mitigate the foggy effect to a certain extent, thereby improving visual clarity. Qualitative experimental results reveal that images processed by UWCNN have a lower contrast, with the most blurred edges and details of the image content, corresponding to the lowest EME scores in qualitative experiments. The contrast of images processed by UDCP and ACDC visually surpasses that of CLAHE and Water-Net. HFM and ASNN offer good contrast and image detail, while IGFU providing more pronounced details and more distinct edges, corresponding to the highest EME scores in qualitative experiments. On the UCIQE metric, the proposed IGFU method scores the highest, surpassing the next best algorithm by 3.71%, 1.43% and 3.19%, respectively, indicating that the algorithm maintains the best balance between hue, saturation and contrast. On the CCF, FDUM and NIQE metrics, the IGFU consistently achieves the best or second-best scores, demonstrating that the processed images have good clarity, colorfulness, appropriate contrast, and high-quality image characteristics. Similarly, on the CEIQE and NIQMC metrics, the IGFU shows commendable performance, confirming that the images have suitable contrast. All in all, the IGFU consistently enhances image quality, restoring color and clarity while preserving visual details.

D. ABLATION STUDY

1) EXPERIMENTAL DESIGN

To evaluate the effectiveness of the proposed IGFU for UIE, relevant ablation experiments were conducted. The IGFU is divided into the following three configurations:

1. Baseline Configuration (BC): Improved GWA.
2. Enhanced Configuration 1 (EC1): Improved GWA+ FFA-Net.
3. Enhanced Configuration 2 (EC2): Improved GWA+ FFA-Net + USM.

The UIEB was selected as the test dataset. By comparing the performance of different configurations, the ablation results were qualitatively and quantitatively analyzed to evaluate image quality and color recovery effects.

2) EXPERIMENTAL RESULT

The image processing results for the UIEB dataset are shown in the following charts, the scores corresponding to optimal image quality are highlighted in bold.

3) EXPERIMENTAL CONCLUSIONS

From the experimental results, it is evident that when applying enhancements solely to underwater images using the improved gray world algorithm, color correction and reduction of chromatic aberrations are achieved effectively. However, the enhancement in image sharpness is not pronounced. In contrast, after incorporating FFA-Net for underwater image dehazing, the underwater veils are removed, significantly improving image clarity, and heightening color contrast reasonably. The addition of USM further enhances image details and edge contours, resulting in clearer and more realistic texture representation of objects within the image. Furthermore, the evaluation metrics consistently improve with the addition of each module, affirming the indispensable role played by each component in enhancing underwater images.

VI. CONCLUSION AND FUTURE WORK

A. CONCLUSION

The traditional GWA effectively corrects the blue and green hues of underwater images but often overcorrects the red hue, leading to distortions in the enhanced image. To address this issue, an iterative processing-based enhanced GWA, referred to as IGFU, is proposed. IGFU specifically categorizes blue and green underwater images, which accurately corrects color bias and significantly reduces overcorrection of the red hue. Subsequently, the color-corrected images were fed into FFA-Net to tackle issues such as haze and low contrast that affect image quality. Aiming at tackling detail and edge blur in underwater images, USM was applied after the defogging operation. Comprehensive experiments demonstrate that the proposed IGFU approach outperforms the state-of-the-art UIE method and exhibits good adaptability under various underwater conditions.

B. FUTURE WORK

Moving forward, to advance the current research further, the main future objectives include:

- Continuous refinement of the method will focus on optimizing parameters and architecture, particularly with FFA-Net and USM, to improve the enhancement effect and increase processing speed.
- Integrating the proposed method as a preprocessing step for target detection involves exploring and assessing its impact and contributions across various target detection methods and its potential for detecting other marine organisms.

- Expanding application scope to enhance underwater video processing. This phase will focus on refining the approach to better suit real-time operation.

REFERENCES

[1] N. Chi, F. T. He, and Z. L. Duan, *Key Technology of Underwater Visible Light Communication [M]*. New Delhi, India: People's Posts and Telecommunications Press, 2020.

[2] N. Singh and A. Bhat, "A systematic review of the methodologies for the processing and enhancement of the underwater images," *Multimedia Tools Appl.*, vol. 82, pp. 38371–38396, 2023.

[3] K. Liao and X. Peng, "Underwater image enhancement using multi-task fusion," *PLoS ONE*, vol. 19, no. 2, 2024, Art. no. e0299110.

[4] N. Yang, "Optimization of image enhancement algorithm based on histogram equalization," M.S. thesis, Dept. Software Eng., Xinjiang Univ., Xinjiang, China, 2021.

[5] S. Muniyappan, A. Allirani, and S. Saraswathi, "A novel approach for image enhancement by using contrast limited adaptive histogram equalization method," in *Proc. 4th Int. Conf. Comput., Commun. Netw. Technol.*, Tiruchengode, India, 2013, pp. 1–6.

[6] G. E. Guraksin, O. Deperlioglu, and U. Kose, "A novel underwater image enhancement approach with wavelet transform supported by differential evolution algorithm," in *Nature Inspired Optimization Techniques for Image Processing Applications, Intelligent Systems Reference Library*, J. Hemanth and V. Balas, Eds., vol. 150, Berlin, Germany: Springer, 2019, ch.11, pp. 255–278.

[7] M. T. Zhou, "White balance underwater image enhancement based on fractional differentiation," *Modern Comput.*, vol. 19, pp. 57–62, 2020.

[8] S. Lin, Z. Li, F. Zheng, Q. Zhao, and S. Li, "Underwater image enhancement based on adaptive color correction and improved retinex algorithm," *IEEE Access*, vol. 11, pp. 27620–27630, 2023.

[9] T. Wang et al., "Research on underwater image enhancement algorithm based on physical model," in *Proc. 3rd Int. Conf. Opt. Commun. Technol.*, Dec. 2023, vol. 129710, pp. 233–239.

[10] I. H. Sarker, "Deep learning: A comprehensive overview on techniques, taxonomy, applications and research directions," *SN Comput. Sci.*, vol. 2, 2021, Art. no. 420.

[11] K. Iqbal, M. Odetayo, A. James, R. A. Salam, and A. Z. Hj Talib, "Enhancing the low quality images using unsupervised colour correction method," in *Proc. 2010 IEEE Int. Conf. Syst., Man Cybern.*, Istanbul, Türkiye, 2010, pp. 1703–1709.

[12] V. Voronin, E. Semenishchev, S. Tokareva, A. Zelenskiy, and S. Agaian, "Underwater image enhancement algorithm based on logarithmic transform histogram matching with spatial equalization," in *Proc. 14th IEEE Int. Conf. Signal Process.*, Beijing, China, 2018, pp. 434–438.

[13] S. K. Tirugatla, V. Anagani, G. Kumar, and V. Ravuri, "Underwater image enhancement using fusion of CLAHE and total generalized variation," *Eng. Lett.*, vol. 31, pp. 1724–1739, 2023.

[14] S. M. An, L. H. Xu, Z. C. Deng, and H. P. Zhang, "HFM: A hybrid fusion method for underwater image enhancement," *Eng. Appl. Artif. Intell. (PA)*, vol. 127, 2024, Art. no. 107219.

[15] Y. C. Yang and H. J. Yun, "An underwater image enhancement method based on color correction and local unsharp masking," *J. Phys., Conf. Ser.*, vol. 2400, 2022, Art. no. 012038.

[16] P. Drews, E. do Nascimento, F. Moraes, S. Botelho, and M. Campos, "Transmission estimation in underwater single images," in *Proc. 2013 IEEE Int. Conf. Comput. Vis. Workshops*, Sydney, NSW, Australia, 2013, pp. 825–830.

[17] T. Y. Li et al., "Underwater image enhancement using adaptive color restoration and dehazing," *Opt. Exp.*, vol. 30, pp. 6216–6235, 2022.

[18] X. K. Mei et al., "UIEOGP: An underwater image enhancement method based on optical geometric properties," *Opt Exp.*, vol. 31, pp. 36638–36655, Oct. 2023.

[19] A. K. Mishra, M. Kumar, and M. S. Choudhry, "Underwater image enhancement by using transmission optimization and background light estimation via principal component analysis fusion," *SIViP*, vol. 18, pp. 3855–3865, 2024.

[20] C. Y. Li, S. Anwar, and P. Fatih, "Underwater scene prior inspired deep underwater image and video enhancement," *Pattern Recognit.*, vol. 98, 2020, Art. no. 107038.

[21] C. Li et al., "An underwater image enhancement benchmark dataset and beyond," *IEEE Trans. Image Process.*, vol. 29, pp. 4376–4389, 2020.

[22] Z. K. Liu, X. X. Fu, C. Lin, and H. Y. Xu, "COC-UFGAN: Underwater image enhancement based on color opponent compensation and dual-subnet underwater fusion generative adversarial network," *J. Vis. Commun. Image Representation*, vol. 100, 2024, Art. no. 104101.

[23] J. Han, J. Zhou, L. Wang, Y. Wang, and Z. Ding, "FE-GAN: Fast and efficient underwater image enhancement model based on conditional GAN," *Electronics*, vol. 12, 2023, Art. no. 1227.

[24] C. W. Park and I. K. Eom, "Underwater image enhancement using adaptive standardization and normalization networks," *Eng. Appl. Artif. Intell.*, vol. 127, no. Part A, Jan. 2024, Art. no. 107445.

[25] C. O. Ancuti, C. Ancuti, C. De Vleeschouwer, and P. Bekaert, "Color balance and fusion for underwater image enhancement," *IEEE Trans. Image Process.*, vol. 27, no. 1, pp. 379–393, Jan. 2018.

[26] X. Qin, Z. Wang, Y. Bai, X. Xie, and H. Jia, "FFA-Net: Feature fusion attention network for single image dehazing," *Proc. AAAI Conf. Artif. Intell.*, vol. 34, no. 07, pp. 11908–11915, 2020.

[27] K. M. He, J. Sun, and X. O. Tang, "Single image haze removal using dark channel prior," in *Proc. 2009 IEEE Conf. Comput. Vis. Pattern Recognit.*, Miami, FL, 2009, pp. 1956–1963.

[28] Shandong Future Robot Co., LTD. Sep. 22, 2023. [Online]. Available: http://www.vvlai.com

[29] C. Ancuti, C. O. Ancuti, T. Haber, and P. Bekaert, "Enhancing underwater images and videos by fusion," in *Proc. 2012 IEEE Conf. Comput. Vis. Pattern Recognit.*, Providence, RI, USA, 2012, pp. 81–88.

[30] C.-Y. Li, J.-C. Guo, R.-M. Cong, Y.-W. Pang, and B. Wang, "Underwater image enhancement by dehazing with minimum information loss and histogram distribution prior," *IEEE Trans. Image Process.*, vol. 25, no. 12, pp. 5664–5677, Dec. 2016.

[31] Y.-T. Peng and P. C. Cosman, "Underwater image restoration based on image blurriness and light absorption," *IEEE Trans. Image Process.*, vol. 26, no. 4, pp. 1579–1594, Apr. 2017.

[32] Y.-T. Peng, K. Cao, and P. C. Cosman, "Generalization of the dark channel prior for single image restoration," *IEEE Trans. Image Process.*, vol. 27, no. 6, pp. 2856–2868, Jun. 2018.

[33] C. Y. Li et al., "A hybrid method for underwater image correction," *Pattern Recognit. Lett.*, vol. 94, pp. 62–67, 2017.

[34] A. Galdran, D. Pardo, A. Picón, and A. Alvarez-Gila, "Automatic red-channel underwater image restoration," *J. Vis. Commun. Image Representation*, vol. 26, pp. 132–145, 2015.

[35] X. Fu, Z. Fan, M. Ling, Y. Huang, and X. Ding, "Two-step approach for single underwater image enhancement," in *Proc. 2017 Int. Symp. Intell. Signal Process. Commun. Syst.*, Xiamen, China, 2017, pp. 789–794.

[36] X. Fu, P. Zhuang, Y. Huang, Y. Liao, X. -P. Zhang, and X. Ding, "A Retinex-based enhancing approach for single underwater image," in *Proc. 2014 IEEE Int. Conf. Image Process.*, Paris, France, 2014, pp. 4572–4576.

[37] P. L. J. Drews, E. R. Nascimento, S. S. C. Botelho, and M. F. Montenegro Campos, "Underwater depth estimation and image restoration based on single images," *IEEE Comput. Graph. Appl.*, vol. 36, no. 2, pp. 24–35, Mar./Apr. 2016.

[38] W. Q. Ren, S. B. Liu, H. Zhang, J.-S. Pan, X. C. Cao, and M.-H. Yang, "Single image dehazing via multi-scale convolutional neural networks," in *Proc. Eur. Conf. Comput. Vis.*, 2016, pp. 154–169.

[39] A. S. Abdul Ghani and N. A. Mat Isa, "Underwater image quality enhancement through integrated color model with Rayleigh distribution," *Appl. Soft Comput.*, vol. 27, pp. 219–230, 2015.

[40] A. S. Abdul Ghani and N. A. Mat Isa, "Enhancement of low quality underwater image through integrated global and local contrast correction," *Appl. Soft Comput.*, vol. 37, pp. 332–344, 2015.

[41] T. He, Z. Zhang, H. Zhang, Z. Zhang, J. Xie, and M. Li, "Bag of tricks for image classification with convolutional neural networks," in *Proc. 2019 IEEE/CVF Conf. Comput. Vis. Pattern Recognit.*, Long Beach, CA, USA, 2019, pp. 558–567.

[42] A. Paszke et al., "Automatic differentiation in pytorch," *Comput. Sci.*, 2017.

[43] P. Karen and G. Artyom, "A new measure of image enhancement," in *Proc. IASTED Int. Conf. Signal Process. Commun.*, 2000, pp. 19–22.

[44] M. Yang and A. Sowmya, "An underwater color image quality evaluation metric," *IEEE Trans. Image Process.*, vol. 24, no. 12, pp. 6062–6071, Dec. 2015.

[45] Y. Wang et al., "An imaging-inspired No-reference underwater color image quality assessment metric," *Comput. Elect. Eng.*, vol. 70, pp. 904–913, 2018.

[46] N. Yang, Q. H. Zhong, K. Li, R. M. Cong, Y. Zhao, and K. Sam, "A reference-free underwater image quality assessment metric in frequency domain," *Signal Process., Image Commun.*, vol. 94, 2021, Art. no. 116218.
[47] A. Mittal, R. Soundararajan, and A. C. Bovik, "Making a 'completely blind' image quality analyzer," *IEEE Signal Process. Lett.*, vol. 20, no. 3, pp. 209–212, Mar. 2013.
[48] L. B. Chang, H. J. Song, M. J. Li, and M. Xiang, "UIDEF: A real-world underwater image dataset and a color-contrast complementary image enhancement framework," *ISPRS J. Photogrammetry Remote Sens.*, vol. 196, pp. 415–428, 2023.
[49] W. Zhang, Y. Wang, and C. Li, "Underwater image enhancement by attenuated color channel correction and detail preserved contrast enhancement," *IEEE J. Ocean. Eng.*, vol. 47, no. 3, pp. 718–735, Jul. 2022.
[50] Y. Fang, K. Ma, Z. Wang, W. Lin, Z. Fang, and G. Zhai, "No-reference quality assessment of contrast-distorted images based on natural scene statistics," *IEEE Signal Process. Lett.*, vol. 22, no. 7, pp. 838–842, Jul. 2015.
[51] K. Gu, W. Lin, G. Zhai, X. Yang, W. Zhang, and C. W. Chen, "No-reference quality metric of contrast-distorted images based on information maximization," *IEEE Trans. Cybern.*, vol. 47, no. 12, pp. 4559–4565, Dec. 2017.
[52] G. Buchsbaum, "A spatial processor model for object color perception," *J. Franklin Inst.-Eng. Appl. Math.*, vol. 310, pp. 1–26, 1980.
[53] Z. Liu, H. Hong, and X. Gao, "Underwater image enhancement based on a combination of improved gated context aggregation network and gray world algorithms," *J. Electron. Imag.*, vol. 33, 2024, Art. no. 013009.
[54] D. Zhu, Z. Liu, and Y. Zhang, "Underwater image enhancement based on colour correction and fusion," *IET Image Process.*, vol. 15, no. 11, pp. 2591–2603, 2021.
[55] C. Li, J. Guo, S. Chen, Y. Tang, Y. Pang, and J. Wang, "Underwater image restoration based on minimum information loss principle and optical properties of underwater imaging," in *Proc. IEEE Int. Conf. Image Process.*, 2016 pp. 1993–1997.
[56] Y. Song, C. Li, S. Xiao, H. Xiao, and B. Guo, "Unsharp masking image enhancement the parallel algorithm based on cross-platform," *Sci. Reports*, vol. 12, 2022, Art. no. 20175.
[57] X. Xu, Y. Cai, X. Liu, C. Liu, and L. Sun, "Improved grey world color correction algorithms," *Acta Photonica Sinica*, vol. 39, pp. 559–564, 2010.
[58] X. Li and J. Wu, "Improved gray world algorithm based on salient detection," in *Advances in Image and Graphics Technologies*, T. Tan, Q. Ruan, X. Chen, H. Ma, and L. Wang, Eds., Berlin, Germany: Springer, 2013, vol. 363, pp. 315–321.
[59] K. H. Sanila, A. A. Balakrishnan, and M. H. Supriya, "Underwater image enhancement using white balance, USM and CLHE," in *Proc. 2019 Int. Symp. Ocean Technol.*, Ernakulam, India, 2019, pp. 106–116.
[60] K. Panetta, C. Gao, and S. Agaian, "Human-Visual-System-inspired underwater image quality measures," *IEEE J. Ocean. Eng.*, vol. 41, no. 3, pp. 541–551, Jul. 2016.

XIN YUAN received the B.Eng. degree in control science and engineering from the Harbin Institute of Technology (HIT), Harbin, China, in 2014, and the M.S. and Ph.D. degrees from Universidad Politécnica de Madrid, Madrid, Spain, in 2018 and 2015, respectively. Her Master and Ph.D. studies are funded by the China Scholarship Council. She is currently an Assistant Professor with the School of Ocean Engineering , HIT. Her research interests include robotic mapping and navigation, object recognition, image processing, and edge intelligence.

CHENHUI WANG is currently working toward the undergraduation degree in robot engineering from the School of Ocean Engineering, Harbin Institute of Technology, Weihai, China. His research interests include image processing and remotely operated vehicle.

XIAOHONG CHEN will graduate from the School of Ocean Engineering, Harbin Institute of Technology Weihai, China, with a bachelor's degree in 2025. Her research interests include underwater image processing and remotely operated Vehicle.

MINGXUAN WANG is currently working toward the undergraduation degree majoring in robot engineering from the Harbin Institute of Technology Weihai, China. His research interests include robot control and image processing.

NING LI (Member, IEEE) received the B.S. and M.S. degrees from Zhengzhou University, Zhengzhou, China, in 2010 and 2014, respectively, and the Ph.D. degree in telematic engineering from Universidad Politécnica de Madrid, Madrid, Spain, in 2018. He is currently an Associate Professor with the School of Computer Science and Technology, Harbin Institute of Technology, Harbin, China. He has authored many journal papers (SCI indexed). His research interests include mobile ad hoc networks, network protocols, topology control, network optimization, and distributed computing.

CHANGLI YU received the B.Eng. and M.S. degrees in naval architecture and ocean engineering from Harbin Engineering University, Harbin, China, and the Ph.D. degree in marine engineering from the University of Ulsan, Ulsan, South Korea, in 2014. He is currently the Dean and an Associate Professor with the School of Ocean Engineering, Harbin Institute of Technology, Harbin. His research interests include assessment of ultimate strength and safety of ships and marine structures, underwater technology and equipment, standardized vessel types for fishing vessels, and noise assessment and control of marine structures.